Hopf Bifurcation for Maps: A Frequency-Domain Approach

María Belén D'Amico, *Student Member, IEEE*, Jorge L. Moiola, *Senior Member, IEEE*, and Eduardo E. Paolini, *Member, IEEE*

***Abstract*—The application of the graphical Hopf theorem (GHT) as a tool for detecting invariant cycles in maps is presented. The invariant cycle emerging from the bifurcation is approximated using an analogous version of the GHT for continuous-time systems. This technique is formulated in the so-called frequency domain and it involves the use of the Nyquist stability criterion and the harmonic balance method. Some examples are included for illustration.**

***Index Terms*—Bifurcation, discrete-time systems, frequency domain, harmonic analysis.**

I. Introduction

THE HOPF bifurcation theorem (HBT) for maps gives conditions for the appearance of an invariant cycle in smooth maps of dimension equal or greater than two when one parameter of the system is varied appropriately [1]. The bifurcation can be supercritical or subcritical, denoting the appearance of stable or unstable cycles for parameter values larger or smaller than the critical one, respectively. The distinction between the vague attractor or the vague repeller at criticality can be obtained by a coordinate transformation leading to a type of standard normal form in polar coordinates. After laborious calculations, it is possible to find an expression for a stability index (the so-called curvature coefficient) that allows to determine which type of bifurcation the system will develop under the variation of the distinguished parameter (see [2], [3] for regular Hopf bifurcations and [4] for applications). The Hopf bifurcation for maps can also be thought as an instrument to describe more complex behavior in continuous-time nonlinear dynamical systems, when the resulting map comes from intersections between a periodic orbit and a certain plane: the so-called Poincaré map. In this case, the bifurcation of the limit cycle results into an invariant torus and the resulting dynamics on the torus: a quasi-periodic motion [5]. This phenomenon has been observed in a variety of electronic and mechanical systems, mainly those having a piecewise linear nonlinearity such as in the very well-known Chua's circuit [6], or in power electronic circuits as in [7], and more recently [8]–[10], as well as for smooth nonlinear vector fields [11], to mention only a few.

This paper presents an adaptation of available formulas for the detection of Hopf bifurcations in continuous-time systems to the case of smooth maps using a frequency-domain approach [12], [13]. The formulas capture the essential asymptotic behavior of the dynamics of the emerging invariant cycle using concepts from control theory. The main formulation and interpretation of the GHT for single-input single-output (SISO) discrete-time systems follow the developments of [14] for continuous-time systems. The extension of this methodology for multiple-input multiple-output (MIMO) systems has been also derived [15]. Based on the simplicity and usefulness of the technique, the multiparameter bifurcation analysis of continuous-time systems [16] may be also extended for discrete-time systems, allowing the study of degenerate Hopf bifurcations for maps (see, for instance, [17] and [18]) via the frequency-domain approach.

The paper is organized as follows. In Section II, the approximation formulas of the invariant cycle emerging through the Hopf bifurcation are derived. In Section III, some examples to illustrate the application of the GHT for maps are shown. Finally, some concluding remarks are given in Section IV.

II. Hopf Bifurcation for Discrete-Time Systems

Let us consider the discrete-time nonlinear system

$$x_{k+1} = Ax_k + Bg(Cx_k;\, \mu) \tag{1}$$

where $x_k, x_{k+1} \in \mathbf{R}^n$, $A \in \mathbf{R}^{n\times n}$, $B \in \mathbf{R}^{n\times l}$, $C \in \mathbf{R}^{m\times n}$, $g(\cdot)$: $\mathbf{R}^m \times \mathbf{R} \to \mathbf{R}^l$ is a smooth (C^r, $r \geq 3$) l-dimensional vector field, $k \in \mathbf{N}$ is the iteration index and $\mu \in \mathbf{R}$ is the bifurcation parameter. All the matrices may have explicit dependence on μ, and A may be the zero matrix.

According to [15], there are many distinct but equivalent feedback representations for (1). This can be easily seen by introducing an arbitrary matrix $D \in \mathbf{R}^{l\times m}$ (which may also depend on μ) and rewriting (1) as

$$\begin{aligned} x_{k+1} &= Ax_k + BDy_k + B[g(y_k;\, \mu) - Dy_k], \\ y_k &= Cx_k. \end{aligned}$$

After applying the z-transform to the previous difference equations, the following frequency-domain representation can be derived

$$G(z;\, \mu) = C[zI - (A + BDC)]^{-1}B \tag{2}$$

Manuscript received October 13, 2000; revised August 31, 2001. This work was supported in part by the Consejo Nacional de Investigaciones Científicas y Técnicas (CONICET) and in part by the Secretaría General de Ciencia y Tecnología at the Universidad Nacional del Sur. The work of J. L. Moiola was supported in part by the Alexander von Humboldt Foundation. This paper was recommended by Associate Editor M. Di Bernardo.

M. B. D'Amico and J. L. Moiola are with the Departamento de Ingeniería Eléctrica, Universidad Nacional del Sur, B8000CPB Bahía Blanca, Argentina. They are also with CONICET Buenos Aires C1033AAJ, Argentina (e-mail: mbdamico@criba.edu.ar).

E. E. Paolini is with the Departamento de Ingeniería Eléctrica, Universidad Nacional del Sur, B8000CPB Bahía Blanca, Argentina.

Publisher Item Identifier S 1057-7122(02)02257-2.

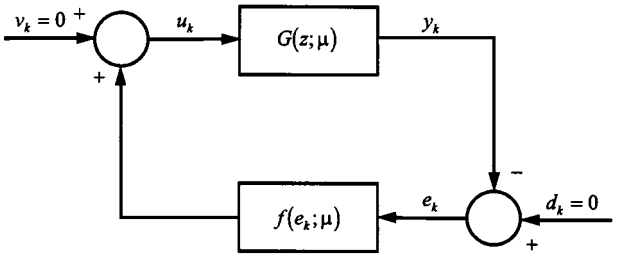

Fig. 1. A nonlinear feedback representation of the system (1).

$$u_k = f(e_k;\,\mu) \doteq g(y_k;\,\mu) - Dy_k, \qquad (3)$$
$$y_k = -e_k.$$

This representation suggests that the discrete-time nonlinear system (1) can be thought as the feedback interconnection shown in Fig. 1, where the linear system $G(\cdot;\cdot)$ and the nonlinear map $f(\cdot;\cdot)$ are defined by (2) and (3), respectively. In the figure, the inputs d_k (generally used to model parameter perturbation, noise effects, etc.) and v_k (external reference input used for nonautonomous systems) are set to zero as in the continuous-time version of the HBT.

The frequency-domain representation has some computational benefits. Observe that $f(\cdot;\cdot)$ is an l-dimensional vector field. Since l is usually smaller than n, it is reasonable to expect that the frequency-domain approach of the HBT requires less amount of computation than its analogous temporal form. For example, the fixed point of (1), obtained by solving a system of n nonlinear equations, now corresponds to the point $\hat{e}$ obtained by solving the system of m nonlinear equations $G(1;\,\mu)\,f(\hat{e};\,\mu) = -\hat{e}$.

Local dynamical behavior can be analyzed via the linearization of the open-loop system, given by $G(z;\,\mu)\,J(\mu)$ where $J(\cdot)$ is the Jacobian matrix, $J = \partial f/\partial e|_{\hat{e}}$. One of the hypotheses of the discrete-time version of the HBT is the crossing of a simple pair of complex eigenvalues through the unit circle for a given value of parameter $\mu = \mu_o$. This is equivalent to the requirement that an eigenvalue of $G(z;\,\mu)\,J(\mu)$ for $z = e^{i\omega}$, denoted as $\hat{\lambda}$, crosses the critical point $-1 + i0$ for some values ω_o and μ_o. This approach is particularly attractive from a feedback systems viewpoint, because the type of bifurcation and the amplitude and frequency of the invariant cycle (in case it does exist) can be derived by simple geometrical arguments on the Nyquist diagram. Moreover, under this approach the study of some failures of the classical hypotheses available for continuous-time systems [16] may be easily extended to the discrete-time case.

A. A Frequency-Domain Approach

The frequency-domain version of the HBT for a SISO discrete-time system can be obtained applying the second-order harmonic balance method [14]. Let us fix μ nearly equal to μ_o so the locus of $\hat{\lambda}(e^{i\omega})$ lies near the critical point $-1+i0$. Therefore, the periodic solutions (if they exist) will have small amplitude and frequency close to ω_o. In this case, it is sufficient to consider

$$e_k = \hat{e} + \mathrm{Re}\left\{a_0 + a_1 e^{i\omega k} + a_2 e^{i2\omega k}\right\} \qquad (4)$$

where $e_k \in \mathbf{R}$ and "Re" means "real part." For simplicity, we can choose the phase of a_1 equal to zero, by properly defining the time origin, so a_2 will be a complex number, $a_2 = |a_2|e^{i\phi}$. We will also assume that $|a_0| = O(|a_1|)^2$, $|a_2| = O(|a_1|)^2$.

Based on the previous hypothesis, $f(\cdot;\,\mu)$ can be expanded in Taylor series in a neighborhood of the fixed point $\hat{e}$. Since we are performing a second-order harmonic approximation, the output of the nonlinear block can be written as

$$f(e_k) = f(\hat{e}) + \mathrm{Re}\left\{A_0 + A_1 e^{i\omega k} + A_2 e^{i2\omega k}\right\}$$

with

$$A_0 = f_1 a_0 + \tfrac{1}{4} f_2 a_1^2$$
$$A_1 = f_1 a_1 + \tfrac{1}{2} f_2 (2a_0 a_1 + a_1 a_2) + \tfrac{1}{8} f_3 a_1^3$$
$$A_2 = f_1 a_2 + \tfrac{1}{4} f_2 a_1^2$$

where f_j denotes $\partial^j f/\partial e^j|_{e=\hat{e}}$.

The linear part of the system should balance input and output harmonics with the corresponding oscillatory solution (4). Therefore, the harmonic balance equations are given by $a_r = -G(e^{ir\omega})A_r$. Solving a_0 and a_2 as function of a_1, we obtain

$$a_0 = -\frac{G(1)}{1 + G(1)f_1}\,\frac{f_2 a_1^2}{4}$$
$$a_2 = -\frac{G(e^{i2\omega})}{1 + G(e^{i2\omega})f_1}\,\frac{f_2 a_1^2}{4}.$$

To avoid singularities it will be assumed that $1 + G(1)f_1 \neq 0$ and that there is no resonance at $e^{i2\omega}$.

Then, defining $H(z) = G(z)/(1 + G(z)f_1)$ and substituting the above expressions into the formula for a_1, the equation involving only a_1 and ω is

$$G(e^{i\omega})f_1 = -1 + a_1^2 \xi(\omega) \qquad (5)$$

where

$$\xi(\omega) = \frac{G(e^{i\omega})}{8}\left[f_2^2(2H(1) + H(e^{i2\omega})) - f_3\right].$$

As we are dealing with a SISO system, the only eigenvalue of the open-loop system is $G(e^{i\omega})f_1$ and thus (5) can be expressed as

$$\hat{\lambda}(e^{i\omega}) = -1 + a_1^2 \xi(\omega). \qquad (6)$$

The previous results have an appealing geometrical interpretation on the Nyquist diagram. Equation (6) can be thought as the intersection between the locus of $\hat{\lambda}(e^{i\omega})$ and a half-line starting at $-1+i0$ in the direction defined by $\xi(\omega)$. If this intersection occurs at $q_R = \hat{\lambda}(e^{i\omega_R})$, then ω_R is the frequency and a_{1R} is the amplitude of the periodic solution. However, ξ is a complex number depending on the unknown frequency of the periodic solution, and therefore (6) is a set of polynomial equations in both a_1 and ω. Although these equations can be solved using iterative methods, a reasonably accurate approximation can be obtained computing ξ for a *fixed* frequency $\tilde{\omega}$ close to ω_R. In this case, if the half-line starting at $-1 + i0$ in the direction defined by $\xi(\tilde{\omega})$ intersects the locus of the eigenvalue at the

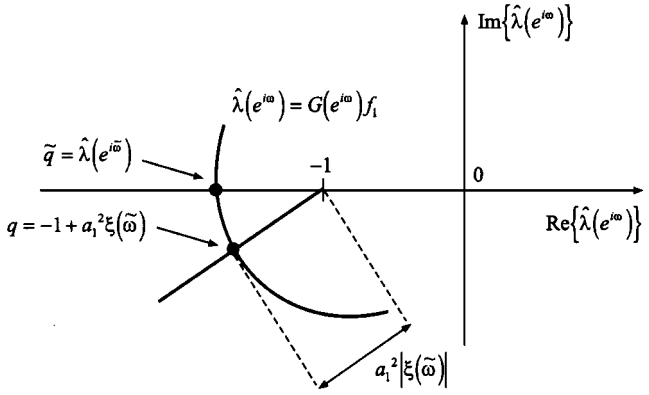

Fig. 2. Geometrical interpretation on the Nyquist diagram of the GHT for a SISO discrete-time system.

point $q = \hat{\lambda}(e^{i\hat{\omega}})$, then $\hat{\omega}$ is the approximate frequency of the periodic solution and $a_1 \approx (|1+q|/|\xi(\tilde{\omega})|)^{1/2}$ its amplitude.

In Section III, we will consider two ways for computing $\tilde{\omega}$. One alternative, as shown in Fig. 2, is to choose $\tilde{\omega}$ as the frequency at which $\hat{\lambda}(e^{i\omega})$ intersects the negative real axis at the point $\tilde{q}$ near -1 (i.e., $\mathrm{Re}\{\hat{\lambda}(e^{i\tilde{\omega}})\}$ is close to -1 and $\mathrm{Im}\{\hat{\lambda}(e^{i\tilde{\omega}})\} = 0$). In that case, $\tilde{\omega}$ depends on the current value of parameter μ. Another option is to consider $\tilde{\omega}$ as the frequency ω_o at which $\hat{\lambda}(e^{i\omega})$ passes over the critical point $-1+i0$ when $\mu = \mu_o$ (i.e., $\tilde{\omega} = \omega_o$ and thus $\mathrm{Re}\{\hat{\lambda}(e^{i\tilde{\omega}})\} = -1$ and $\mathrm{Im}\{\hat{\lambda}(e^{i\tilde{\omega}})\} = 0$). This value of $\tilde{\omega}$ is then used as an approximation for all values of μ taking into account the general (local) linear law of the variation of the frequency versus the bifurcation parameter for regular Hopf bifurcations.

B. MIMO Systems

The previous computations for SISO discrete-time systems can be extended to MIMO systems. The procedure is completely similar to the one given in [15]. We suppose that the second-order harmonic balance solution is now

$$e_k = \hat{e} + \mathrm{Re}\left\{\sum_{r=0}^{2} E^r e^{ir\omega k}\right\} \tag{7}$$

where $e_k \in \mathbf{R}^m$ and $E^r \in \mathbf{C}^m$. The coefficient vectors E^r are obtained equating the output of the linear part with the input signal to the nonlinear feedback vector field $f(\cdot;\cdot)$, whose Fourier coefficient vectors are noted as F^r. Thus, the harmonic balance equations are $E^r = -G(e^{ir\omega})F^r$. These equations are solved in terms of $E^1 = \theta v$, where v is the normalized right eigenvector associated with the eigenvalue $\hat{\lambda}(e^{i\omega})$, and θ is the measure of the amplitude of the periodic solution. The other complex vectors are given by $E^0 = \theta^2 v^0$ and $E^2 = \theta^2 v^2$ with

$$v^0 = -\tfrac{1}{4} H(1) Q\overline{v}$$
$$v^2 = -\tfrac{1}{4} H(e^{i2\omega}) Q v$$

where $H(z) \doteq (1+G(z)J)^{-1}G(z)$, "$-$" is the complex conjugate operator and $Q \in \mathbf{R}^{l\times m}$ involves the second-order partial derivatives of $f(\cdot;\cdot)$ with respect to e_k and it can be computed as in [15].

Therefore, for the periodic solution (7) to exist, it is necessary that

$$\hat{\lambda}(e^{i\omega}) = -1 + \theta^2 \xi(\omega) \tag{8}$$

with

$$\xi(\omega) = -u^T G(e^{i\omega}) p(\omega, v)$$

where $p(\omega, v) = Qv^0 + 1/2\overline{Q}v^2 + 1/8L\overline{v}$, u is the normalized left eigenvector associated with the eigenvalue $\hat{\lambda}(e^{i\omega})$ and $L \in \mathbf{R}^{l\times m}$, involving the third-order partial derivatives of $f(\cdot;\cdot)$ with respect to e_k, can be computed as in [15]. Since (8) can be thought as the MIMO system counterpart of (6), an analogous geometrical interpretation can be applied.

III. Applications of the GHT in Maps

In this section, the dynamical behavior of several smooth maps is studied using the methodology proposed above. Example 1 shows a detailed analysis of the well-known delayed logistic map, and Example 2 presents the derivation of an approximate expression of the periodic oscillation in a neural netlet. In both cases, the discrete-time system develops a supercritical Hopf bifurcation. On the other hand, Example 3 describes the appearance of a subcritical Hopf bifurcation in an adaptively-controlled system, showing also how the GHT can be used to estimate the boundary of the basin of attraction of a fixed point.

Example 1: The delayed logistic map is given by

$$\begin{cases} x_{k+1}^1 = x_k^2 \\ x_{k+1}^2 = \mu x_k^2 \left(1 - x_k^1\right). \end{cases} \tag{9}$$

This system has two fixed points: the origin which is stable for $0 < \mu < 1$ and unstable for $\mu \geq 1$; and $(1-\mu^{-1}, 1-\mu^{-1})$ which is unstable for $0 < \mu < 1$ and stable for $1 < \mu < \mu_o = 2$. For $\mu = \mu_o$, the two eigenvalues associated to the latter point are complex conjugated and lie on the unit circle. When the parameter μ takes values greater than μ_o, these eigenvalues cross the unit circle from the inside to the outside, changing the stability of the fixed point.

It is well-known that (9) develops a supercritical Hopf bifurcation around the nonzero fixed point (see [1] for a one-parameter analysis, and [19] for a more complete two-parameter study). In this work, we emphasize the approximation of the invariant cycle instead of the computation of the resonant behavior of the system. The interested readers should consult [19] to find more details when the invariant cycle can lose its smoothness through homoclinic and heteroclinic interactions.

In order to apply the GHT, the map (9) can be transformed into the equivalent feedback system (2) and (3) choosing the trivial representation

$$A = \begin{bmatrix} 0 & 1 \\ 0 & \mu \end{bmatrix} \quad B = \begin{bmatrix} 0 \\ 1 \end{bmatrix} \quad C = \begin{bmatrix} 1 & 0 \\ 0 & 1 \end{bmatrix}$$
$$D = [0 \quad 0], \quad g(y_k;\mu) = -\mu y_k^1 y_k^2.$$

Then

$$G(z;\mu)=\frac{1}{z-\mu}\begin{bmatrix}z^{-1}\\1\end{bmatrix},\qquad f(e_k;\mu)=-\mu e_k^1 e_k^2.$$

Linearizing the nonlinear map $f(e_k;\mu)$ around the fixed point $\hat{e}=(-1+\mu^{-1},-1+\mu^{-1})$, the Jacobian matrix is given by $J(\mu)=(\mu-1,\mu-1)$ and thus the open-loop system matrix is

$$G(z;\mu)J(\mu)=\frac{\mu-1}{z-\mu}\begin{bmatrix}z^{-1}&z^{-1}\\1&1\end{bmatrix}$$

with eigenvalues

$$\lambda_1(e^{i\omega})=0$$
$$\lambda_2(e^{i\omega})=(\mu-1)\frac{1+e^{-i\omega}}{e^{i\omega}-\mu}.$$

The only relevant eigenvalue is $\lambda_2(e^{i\omega})$, as $\lambda_1(e^{i\omega})\equiv 0$ for all ω and thus it never crosses the critical point $-1+i0$. Therefore, $\lambda_2(e^{i\omega})$ corresponds to the eigenvalue $\hat{\lambda}(e^{i\omega})$ defined previously.

The normalized right and left eigenvectors associated with $\lambda_2(e^{i\omega})$ are

$$v=\frac{\sqrt{2}}{2}\begin{bmatrix}e^{-i\omega}\\1\end{bmatrix}\quad u=\frac{\sqrt{2}}{2}\begin{bmatrix}1\\1\end{bmatrix}.$$

The matrices Q and L (computed as in [15]) are

$$Q=-\frac{\sqrt{2}\mu}{2}\begin{bmatrix}1&e^{-i\omega}\end{bmatrix}\quad L=\begin{bmatrix}0&0\end{bmatrix}$$

and the linearized closed-loop matrix is

$$H(z)=\frac{1}{\mu-1-z+z^2}\begin{bmatrix}1\\z\end{bmatrix}.$$

Then

$$v^o=\hat{v}^o(\omega)\begin{bmatrix}1\\1\end{bmatrix}\quad v^2=\hat{v}^2(\omega)\begin{bmatrix}1\\e^{i2\omega}\end{bmatrix}$$

where

$$\hat{v}^o(\omega)=\frac{\mu}{8(\mu-1)}\left(e^{i\omega}+e^{-i\omega}\right)$$
$$\hat{v}^2(\omega)=\frac{\mu e^{-i\omega}}{4(\mu-1-e^{i2\omega}+e^{i4\omega})}$$

and thus

$$\xi(\omega)=\frac{p(\omega)}{\sqrt{2}(\mu-e^{-i\omega})}$$

with

$$p(\omega)=-\frac{\sqrt{2}\mu}{4}\left[2\hat{v}^o(\omega)(1+e^{-i\omega})+\hat{v}^2(\omega)(e^{i3\omega}+1)\right].$$

Assuming, for instance, that $\mu=2.05$, the intersection between $\lambda_2\left(e^{i\omega}\right)$ and the negative real axis near the critical point $-1+i0$ takes place at $\tilde{\omega}=1.018$ and thus $\xi(\tilde{\omega})=-0.5185-i0.0118$. The locus of $\lambda_2(e^{i\omega})$ and the half-line starting at $-1+i0$ in the direction defined by $\xi(\tilde{\omega})$ are shown in Fig. 3. As expected, the locus intersects the half-line verifying the existence of an invariant cycle. This intersection occurs at $q=-1.05-i0.0012$ and the corresponding frequency is $\hat{\omega}=1.016$. The amplitude of the approximate periodic solution is obtained as

$$\theta=\sqrt{\frac{|1+q|}{|\xi(\tilde{\omega})|}}=0.310\,54$$

and then the first three harmonics are

$$E^0=0.024\,79\begin{bmatrix}1\\1\end{bmatrix}$$
$$E^1=0.219\,58\begin{bmatrix}e^{i5.267}\\1\end{bmatrix}$$
$$E^2=0.025\,83\begin{bmatrix}e^{i0.701}\\e^{i2.102}\end{bmatrix}.$$

The invariant cycle predicted through the GHT and that obtained by numerical simulation are depicted in Fig. 4. As can be seen in the figure, there exists a close agreement between the actual and the predicted cycles because the parameter μ is close to the critical value μ_o.

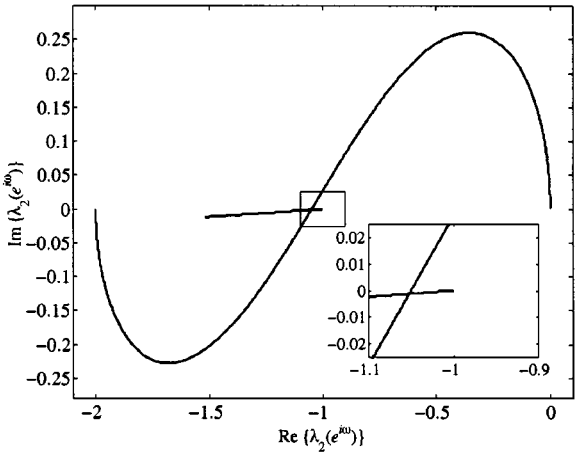

Fig. 3. The locus of $\lambda_2(e^{i\omega})$ and the half-line $-1+\theta^2\xi(\tilde{\omega})$.

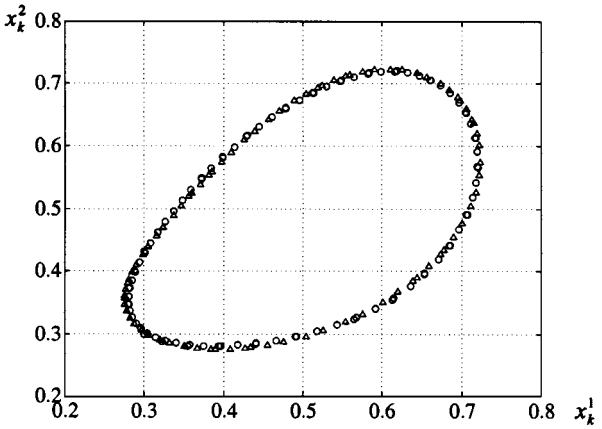

Fig. 4. The stable invariant cycles predicted via the GHT (△) and by simulation (○).

Example 2: The discretized model of a neural netlet of excitation and inhibition is

$$\begin{cases} x_{k+1}^1 = e^{-\mu}x_k^1 + a(1-e^{-\mu})\tanh(c_1 x_k^2) \\ x_{k+1}^2 = e^{-\mu}x_k^2 + a(1-e^{-\mu})\tanh(-c_2 x_k^1) \end{cases} \tag{10}$$

where a, c_1 and c_2 are positive constants and μ is the bifurcation parameter that represents the time-delay due to the finite switching speed of amplifiers in models of electronic networks [4]. For oscillations to exist, $a^2c_1c_2 > 1$.

The origin is the only fixed point of (10) and it is stable for $0 < \mu < \mu_o$ with $\mu_o = \ln(a^2c_1c_2+1) - \ln(a^2c_1c_2-1)$. When $\mu = \mu_o$, the linear part of the map has a pair of complex conjugate eigenvalues on the unit circle. As the parameter μ is increased through μ_o, these eigenvalues cross the unit circle modifying the stability of the fixed point.

A representation leading to a single nontrivial eigenlocus is given by the matrices

$$A = \begin{bmatrix} e^{-\mu} & 0 \\ 0 & e^{-\mu} \end{bmatrix} \quad B = C = \begin{bmatrix} 1 & 0 \\ 0 & 1 \end{bmatrix} \quad D = \begin{bmatrix} \alpha & 0 \\ 0 & \beta \end{bmatrix}$$

and the vector

$$g(y_k;\,\mu) = a(1-e^{-\mu})\begin{bmatrix} \tanh(c_1 y_k^2) \\ \tanh(-c_2 y_k^1) \end{bmatrix}$$

with $\alpha\beta = -a^2c_1c_2(1-e^{-\mu})^2$. Then

$$G(z;\,\mu) = \begin{bmatrix} \dfrac{1}{z-(e^{-\mu}+\alpha)} & 0 \\ 0 & \dfrac{1}{z-(e^{-\mu}+\beta)} \end{bmatrix}$$

$$f(e_k;\,\mu) = \begin{bmatrix} a(1-e^{-\mu})\tanh(-c_1 e_k^2) + \alpha e_k^1 \\ a(1-e^{-\mu})\tanh(c_2 e_k^1) + \beta e_k^2 \end{bmatrix}.$$

The open-loop system matrix is

$$G(z;\,\mu)J(\mu) = \begin{bmatrix} \dfrac{\alpha}{z-(e^{-\mu}+\alpha)} & \dfrac{-ac_1(1-e^{-\mu})}{z-(e^{-\mu}+\alpha)} \\ \dfrac{ac_2(1-e^{-\mu})}{z-(e^{-\mu}+\beta)} & \dfrac{\beta}{z-(e^{-\mu}+\beta)} \end{bmatrix}$$

and its eigenvalues are

$$\lambda_1(e^{i\omega}) = 0,$$

$$\lambda_2(e^{i\omega}) = \frac{(\alpha+\beta)(e^{i\omega}-e^{-\mu}) - 2\alpha\beta}{[e^{i\omega}-(e^{-\mu}+\alpha)][e^{i\omega}-(e^{-\mu}+\beta)]}.$$

As expected, the only relevant eigenvalue is $\lambda_2(e^{i\omega})$, so $\hat{\lambda}(e^{i\omega}) = \lambda_2(e^{i\omega})$.

The normalized right and left eigenvectors associated with $\lambda_2(e^{i\omega})$ are

$$v = \left(1+|\hat{v}(\omega)|^2\right)^{-1/2}\begin{bmatrix} \hat{v}(\omega) \\ 1 \end{bmatrix}$$

$$u = \left(1+|\hat{u}|^2\right)^{-1/2}\begin{bmatrix} \hat{u} \\ 1 \end{bmatrix}$$

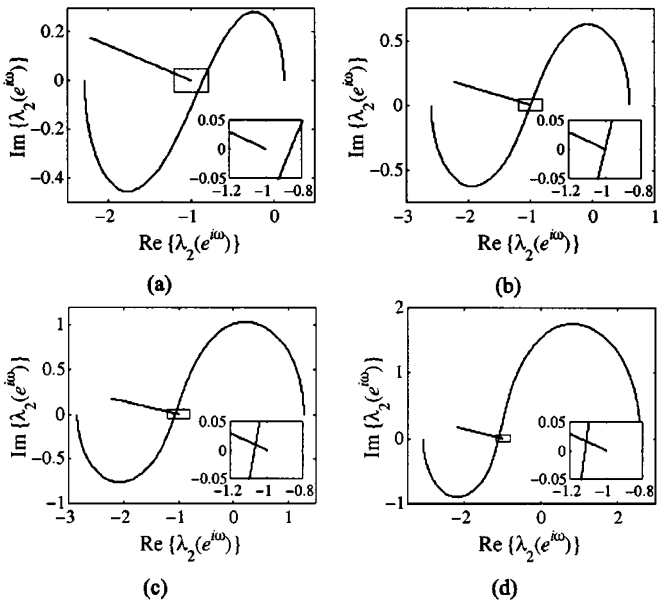

Fig. 5. The locus of $\lambda_2(e^{i\omega})$ and the half-line $-1+\theta^2\xi(\tilde{\omega})$ for different values of μ. (a) $\mu = 0.55$. (b) $\mu = \mu_o$. (c) $\mu = 0.8$. (d) $\mu = 0.9$.

with $\hat{u} = ac_2(1-e^{-\mu})$ and

$$\hat{v}(\omega) = -\frac{ac_1(1-e^{-\mu})[e^{i\omega}-(e^{-\mu}+\beta)]}{\beta[e^{i\omega}-(e^{-\mu}+\alpha)]}.$$

In this example, the matrices Q and L are

$$Q = \begin{bmatrix} 0 & 0 \\ 0 & 0 \end{bmatrix},$$

$$L = \frac{2ac_1^3(1-e^{-\mu})}{1+|\hat{v}(\omega)|^2}\begin{bmatrix} 0 & 1 \\ -\left(\dfrac{c_2}{c_1}\right)^3\hat{v}(\omega)^2 & 0 \end{bmatrix}$$

and then,

$$\xi(\omega) = \frac{\alpha\beta(c_1^2+c_2^2|\hat{v}(\omega)|)^2}{4(1+|\hat{v}(\omega)|^2)^2\left[(\alpha+\beta)(e^{i\omega}-e^{-\mu})-2\alpha\beta\right]}.$$

To simplify the calculations, we choose $c_1 = c_2 = \beta = 1$, $a = \sqrt{3}$ and assume that $\tilde{\omega} = \omega_o = 1.046$ for all values of the parameter μ. The locus of $\lambda_2(e^{i\omega})$ and the half-line from the point $-1+i0$ in the direction of $\xi(\tilde{\omega})$ corresponding to different values of μ are shown in Fig. 5. For $\mu < \mu_o = \ln 2$, the fixed point is stable and there is no intersection between the locus of the eigenvalue and the half-line [Fig. 5(a)]. As μ increases, the locus moves away from criticality [Fig. 5(b)] and intersects the half-line. Then, for $\mu > \mu_o$ the fixed point is unstable and an intersection appears denoting the existence of an invariant cycle [Fig. 5(c) and (d)]. Moreover, a stability analysis for small perturbations of the intersection point establishes that the cycle is stable (for more details, see [15]).

From (7), the expression of the periodic solution is

$$\begin{cases} x_k^1 \cong \rho(\hat{\omega})(\mathrm{Re}\{\hat{v}(\hat{\omega})\}\cos(\hat{\omega}k) - \mathrm{Im}\{\hat{v}(\hat{\omega})\}\sin(\hat{\omega}k)) \\ x_k^2 \cong \rho(\hat{\omega})\cos(\hat{\omega}k) \end{cases}$$

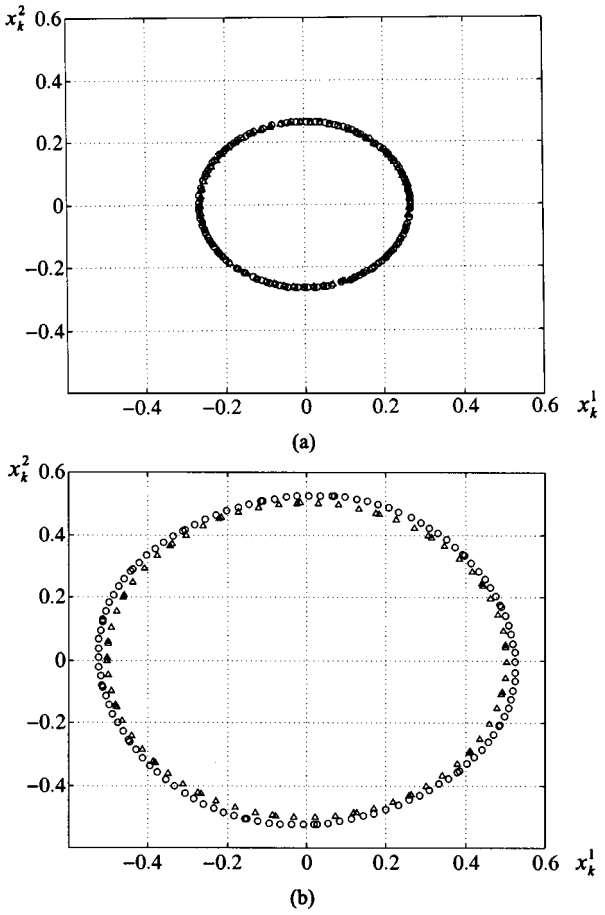

Fig. 6. Stable invariant cycles computed by the GHT (△) and by simulation (○) for different values of μ. (a) $\mu = 0.72$. (b) $\mu = 0.8$.

with $\rho(\hat{\omega}) = -\theta(1 + |\hat{v}(\hat{\omega})|^2)^{-1/2}$. Since $\hat{v}(\hat{\omega}) \simeq i$ for μ near μ_o, the last equation can be approximated as

$$\begin{cases} x_k^1 \cong \dfrac{\sqrt{2}}{2}\,\theta \sin(\hat{\omega}k) \\ x_k^2 \cong -\dfrac{\sqrt{2}}{2}\,\theta \cos(\hat{\omega}k). \end{cases}$$

The invariant cycles obtained through the GHT and those obtained iterating the map are shown in Fig. 6. In Fig. 6(a) the parameter μ is near the critical value μ_o ($\mu = 0.72$) and thus the actual and the predicted cycles are very similar. For larger values of μ ($\mu = 0.8$, for example) the difference between both cycles increases [see Fig. 6(b)], revealing the local nature of the approximation.

Example 3: In the adaptively-controlled system proposed in [17], the aim is to maintain a linear, second-order discrete-time system at a desired state using a first-order model-reference, self-adapting, nonlinear feedback control scheme. The map including the plant, the controller and the estimator is

$$\begin{cases} x_{k+1}^1 = x_k^2 \\ x_{k+1}^2 = \mu x_k^1 + a + x_k^2 x_k^3 \\ x_{k+1}^3 = x_k^3 - \dfrac{a x_k^2(\mu x_k^1 + a - 1 + x_k^2 x_k^3)}{c + (x_k^2)^2} \end{cases} \tag{11}$$

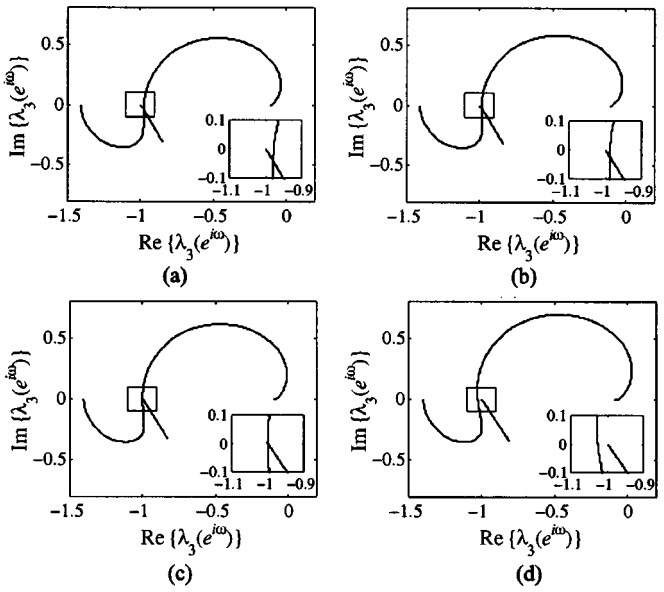

Fig. 7. The locus of $\lambda_3(e^{i\omega})$ and the half-line $-1+\theta^2\xi(\bar{\omega})$ for different values of μ. (a) $\mu = -0.5$. (b) $\mu = -0.51$. (c) $\mu = -0.5238$. (d) $\mu = -0.55$.

where c is a small positive constant of the estimation algorithm and a and μ (k and b in [17], respectively) are parameters that define the mismatch between the plant and the model-reference. This system presents a complex dynamical behavior in the neighborhood of its unique fixed point $(1,\ 1,\ 1-\mu-a)$ when varying a and μ (see [17]). We will focus our attention in the region of the $(a,\ \mu)$-plane where this point loses local stability via a Hopf bifurcation.

To apply the GHT, the map (11) is expressed as a feedback system adopting

$$A = \begin{bmatrix} 0 & 1 & 0 \\ \mu & 0 & 0 \\ 0 & 0 & 1 \end{bmatrix} \quad B = \begin{bmatrix} 0 & 0 \\ 1 & 0 \\ 0 & 1 \end{bmatrix}$$

$$C = \begin{bmatrix} 1 & 0 & 0 \\ 0 & 1 & 0 \\ 0 & 0 & 1 \end{bmatrix} \quad D = \begin{bmatrix} 0 & 0 & 0 \\ -\mu\alpha_2 & -\alpha_1 & 1 \end{bmatrix}$$

$$g(y_k;\cdot) = \begin{bmatrix} a + y_k^2 y_k^3 \\ \dfrac{-a y_k^2\left[\mu(y_k^1 - 1) + \alpha_1 + y_k^2 y_k^3\right]}{c + (y_k^2)^2} \end{bmatrix}$$

where $\alpha_1 = \mu + a - 1$ and $\alpha_2 = a(c+1)^{-1}$. Then

$$G(z;\cdot) = \frac{1}{z^2 - \mu} \begin{bmatrix} 1 & 0 \\ z & 0 \\ -\dfrac{\mu\alpha_2 + \alpha_1 z}{z-2} & \dfrac{z^2 - \mu}{z-2} \end{bmatrix}$$

$$f(e_k;\cdot) = g(-e_k;\cdot) - \begin{bmatrix} 0 \\ \mu\alpha_2 e_k^1 + \alpha_1 e_k^2 - e_k^3 \end{bmatrix}.$$

The eigenvalues of the open-loop matrix $G(z;\cdot)J(\cdot)$ are

$$\lambda_1\left(e^{i\omega}\right) = \lambda_2(e^{i\omega}) = 0,$$

$$\lambda_3(e^{i\omega}) = \frac{(1 + \alpha_1 + \alpha_2)e^{i2\omega} - \alpha_1 e^{i\omega} - \mu}{(e^{i2\omega} - \mu)(e^{i\omega} - 2)}.$$

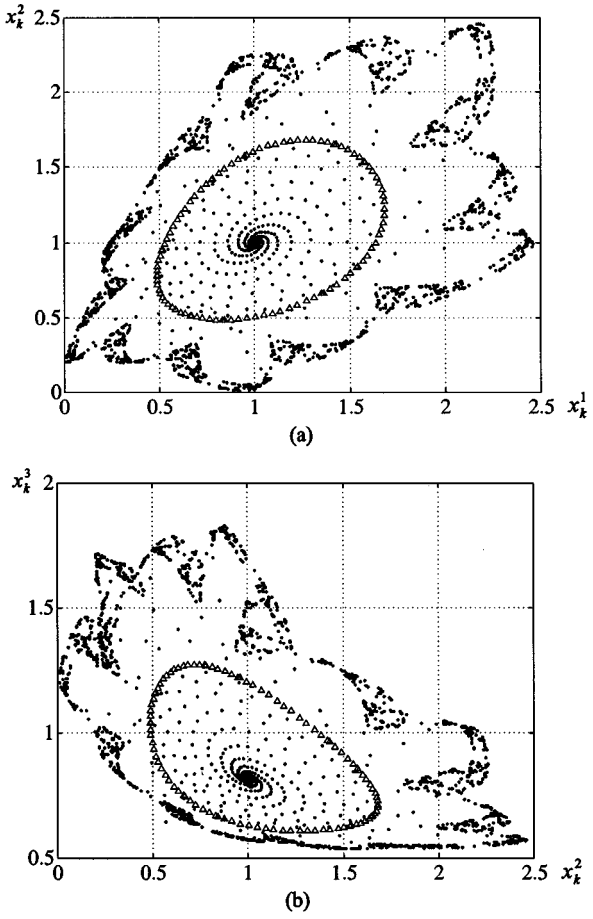

Fig. 8. Projections of the unstable cycle obtained by the GHT (△) and trajectories of the map (∘) for $\mu = -0.5$.

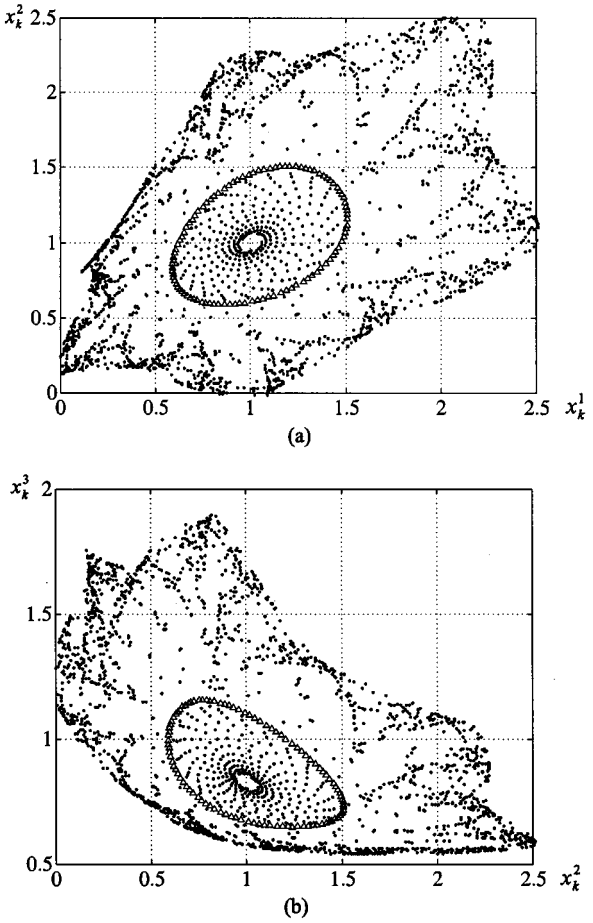

Fig. 9. Projections of the unstable cycle obtained by the GHT (△) and trajectories of the map (∘) for $\mu = -0.51$.

Notice that, as in the previous examples, an appropriate election of the feedback representation leads to a single nontrivial eigenvalue, $\hat{\lambda}(e^{i\omega}) = \lambda_3(e^{i\omega})$.

A necessary condition for a Hopf bifurcation is given by $a^2 + 4\mu_o a < 0$ with $\mu_o = -(c+1)/(c+2)$ (see [17]). In order to compute some numerical results, we choose $c = 0.1$, $a = 0.68$, assuming μ as the main bifurcation parameter.

The locus of $\lambda_3(e^{i\omega})$ and the half-line $-1 + \theta^2\xi(\tilde{\omega})$ for different values of μ are presented in Fig. 7. When μ is greater than the critical value μ_o [Fig. 7(c)], the fixed point is stable and an unstable invariant cycle is detected [Fig. 7(a) and (b)], while for $\mu < \mu_o$ the fixed point is unstable and no invariant cycle exists [Fig. 7(d)]. Therefore, the map (11) develops a subcritical Hopf bifurcation.

Figs. 8 and 9 show projections on the phase planes (x_k^1, x_k^2) and (x_k^2, x_k^3) of the unstable invariant cycles obtained by the GHT, and some trajectories of the adaptively-controlled system. The initial conditions are located inside and outside the cycle, and the simulations have been performed for values of μ greater than μ_o. As can be seen in the figures, when the parameter μ is closer to μ_o, the invariant cycle is smaller.

An useful byproduct of the frequency-domain analysis is also depicted in Figs. 8 and 9. System (11) has two attractors at this parameter setting: the stable fixed point and a chaotic attractor, with the unstable invariant cycle (and its stable manifold when the third contracting direction is taken into account) defining the boundary of attraction of the fixed point. Notice that this cycle, due to its saddle-node nature in $\mathbf{R}^3$ [17], can not be located numerically by backward iteration of the map in time. Consequently, the predictions of the GHT method complete the results of [17] giving an explicit estimation of the emerging invariant cycle.

IV. Conclusions

A frequency-domain approach to analyze Hopf bifurcations for smooth maps as well as approximation formulas to recover the invariant cycle using a second-order harmonic balance technique have been presented. The application of the GHT is illustrated with three examples. A close agreement between the numerical simulations and the approximate solution is obtained when the parameter is close to the bifurcation point. Since the GHT for discrete-time systems provides a useful graphical interpretation, an extension to deal with other degenerate cases seems very attractive to pursue.

Acknowledgment

One of the authors, J. L. Moiola acknowledges the hospitality of the University of Cologne, Cologne, Germany.

REFERENCES

[1] J. Hale and H. Koçak, *Dynamics and Bifurcations*. New York: Springer Verlag, 1991.

[2] P. Glendinning, *Stability, Instability and Chaos. An Introduction to the Theory of Nonlinear Differential Equations*. Cambridge, U.K.: Cambridge Univ. Press, 1994.

[3] Y. H. Wang, "Computations of the stability condition for the Hopf bifurcation of diffeomorphisms on $\mathbf{R}^2$," *SIAM J. Appl. Math.*, vol. 34, no. 3, pp. 167–175, 1978.

[4] K. Gopalsamy and I. Leung, "Delay induced periodicity in a neural netlet of excitation and inhibition," *Physica D*, vol. 89, no. <3/4, pp. 395–426, 1996.

[5] Y. A. Kuznetsov, *Elements of Applied Bifurcation Theory*. New York: Springer Verlag, 1995.

[6] L. O. Chua, C. W. Wu, A. Huang, and G.-Q. Zhong, "A universal circuit for studying and generating chaos—Part I: Routes to chaos," *IEEE Trans. Circuits Syst. I*, vol. 40, pp. 732–744, Oct. 1993.

[7] J. H. B. Deane and D. C. Hamill, "Instability, subharmonics, and chaos in power electronic systems," *IEEE Trans. Power Electron.*, vol. 5, pp. 260–268, July 1990.

[8] W. C. Y. Chan and C. K. Tse, "Study of bifurcations in current-programmed DC–DC boost converters: From quasi-periodicity to period-doubling," *IEEE Trans. Circuits Syst. I*, vol. 44, pp. 1129–1142, Dec. 1997.

[9] A. E. Aroudi, L. Venadero, E. Toribio, and G. Olivar, "Hopf bifurcation and chaos from torus breakdown in a PWM voltage-controlled DC–DC boost converter," *IEEE Trans. Circuits Syst. I*, vol. 46, pp. 1374–1382, Nov. 1999.

[10] C. K. Tse, Y. M. Lai, and H. H. C. Iu, "Hopf bifurcation and chaos in a free-running current-controlled Ćuk switching regulator," *IEEE Trans. Circuits Syst. I*, vol. 47, pp. 448–457, Apr. 2000.

[11] Q. Bi and P. Yu, "Double Hopf bifurcations and chaos of a nonlinear vibration system," *Nonlinear Dynamics*, vol. 19, no. 4, pp. 313–332, 1999.

[12] M. B. D'Amico, J. L. Moiola, and E. E. Paolini, "Hopf bifurcations in discrete-time systems via a frequency-domain approach," in *Proc. Int. Conf. 'Control of Oscillations and Chaos' (COC'2000)*, vol. 2, St. Petersburg, Russia, 2000, pp. 290–293.

[13] ——, "Hopf bifurcation for maps in neuronal nets," in *Proc. Workshop on Nonlinear Dynamics of Electronic Systems (NDES'2000)*, Catania, Italy, 2000, pp. 90–94.

[14] D. J. Allwright, "Harmonic balance and the Hopf bifurcation theorem," *Math. Proc. Cambridge Phil. Soc.*, vol. 82, no. 3, pp. 453–467, 1977.

[15] A. I. Mees and L. O. Chua, "The Hopf bifurcation theorem and its applications to nonlinear oscillations in circuits and systems," *IEEE Trans. Circuits Syst.*, vol. CAS-26, pp. 235–254, Apr. 1979.

[16] J. L. Moiola and G. Chen, *Hopf Bifurcation Analysis: A Frequency Domain Approach*, ser. Series A, World Sci. Series on Nonlinear Science. Singapore: World Scientific , 1996, vol. 21.

[17] C. E. Frouzakis, R. A. Adomaitis, and I. G. Kevrekidis, "Resonance phenomena in an adaptively-controlled system," *Int. J. Bifurcation and Chaos*, vol. 1, no. 1, pp. 83–106, 1991.

[18] B. B. Peckham, C. E. Frouzakis, and I. G. Kevrekidis, "Bananas and banana splits: A parametric degeneracy in the Hopf bifurcation for maps," *SIAM J. Math. Anal.*, vol. 26, no. 1, pp. 190–217, 1995.

[19] D. G. Aronson, M. A. Chory, G. R. Hall, and R. P. McGehee, "Bifurcations from an invariant circle for two-parameter families of maps of the plane: A computer-assisted study," *Commun. Math. Phys.*, vol. 83, no. 3, pp. 303–354, 1982.

María Belén D'Amico (S'98) was born in Río Grande, Argentina, on October 30, 1973. She received the B.S. degree in electronic engineering from the Universidad Nacional del Sur, Bahía Blanca, Argentina, in 1999.

Since 1998, she has been with the Control group of the Departamento de Ingeniería Eléctrica at the Universidad Nacional del Sur. Her research interests are in the field of the analysis of nonlinear circuits and systems.

Jorge L. Moiola (S'86–M'92–SM'98) was born in Rosario, Argentina, on August 3, 1961. He received the B.S. degree in electrical engineering from the Universidad Nacional del Sur (UNS), Bahía Blanca, Argentina, in 1986, the M.Sc. degree in electrical engineering from the University of Houston (UH), Houston, TX, in 1991, and the Ph.D. degree in control systems from the UNS, in 1992.

Since then he has been with the Departamento de Ingeniería Eléctrica at the UNS, where he is currently Associate Professor and a member of the CONICET (Consejo Nacional de Investigaciones Científicas y Técnicas). In 1995, he was with the Department of Electrical and Computer Engineering at UH, as a visiting scholar, and in the Spring of 1998 at the University of California, Berkeley, as a Fulbright Scholar. Since 2001, he is a Research Scholar of the Alexander von Humboldt Foundation with the University of Cologne, Cologne, Germany.

He is the Editor-in-Chief of the Latin American Applied Research Journal. His primary research interest is in the field of nonlinear oscillations and bifurcations related to control systems theory.

Eduardo E. Paolini (M'00) was born in Punta Alta, Argentina, on March 12, 1963. He received the B.S. degree in electrical engineering from the Universidad Nacional del Sur, Bahía Blanca, Argentina, in 1987. Since then, he has been with the Departamento de Ingeniería Eléctrica at the Universidad Nacional del Sur. His research interests are nonlinear systems theory and its applications.